Size- and temperature-dependent magnetization of iron nanoclusters

G. Dos Santos [1,2,*] R. Aparicio,[1,2] D. Linares,[3] E. N. Miranda,[4] J. Tranchida,[5] G. M. Pastor,[6] and E. M. Bringa [1,2,7]

[1]*CONICET, Mendoza 5500, Argentina*
[2]*Facultad de Ingeniería, Universidad de Mendoza, Mendoza 5500, Argentina*
[3]*Departamento de Física, Instituto de Física Aplicada, Universidad Nacional de San Luis-CONICET, Ejército de Los Andes 950,*
D5700HHW San Luis, Argentina
[4]*IANIGLA-CONICET, CCT Mendoza, 5500-Mendoza, Argentina*
[5]*Computational Multiscale, Center for Computing Research, Sandia National Laboratories, P.O. Box 5800, MS 1322, Albuquerque, New*
Mexico 87185, USA
[6]*Institute of Theoretical Physics, University of Kassel, 34134 Kassel, Germany*
[7]*Centro de Nanotecnología Aplicada, Facultad de Ciencias, Universidad Mayor, Santiago 8580745, Chile*

The magnetic behavior of bcc iron nanoclusters, with diameters between 2 and 8 nm, is investigated by means of spin dynamics simulations coupled to molecular dynamics, using a distance-dependent exchange interaction. Finite-size effects in the total magnetization as well as the influence of the free surface and the surface/core proportion of the nanoclusters are analyzed in detail for a wide temperature range, going beyond the cluster and bulk Curie temperatures. Comparison is made with experimental data and with theoretical models based on the mean-field Ising model adapted to small clusters, and taking into account the influence of low coordinated spins at free surfaces. Our results for the temperature dependence of the average magnetization per atom $M(T)$, including the thermalization of the transnational lattice degrees of freedom, are in very good agreement with available experimental measurements on small Fe nanoclusters. In contrast, significant discrepancies with experiment are observed if the translational degrees of freedom are artificially frozen. The finite-size effects on $M(T)$ are found to be particularly important near the cluster Curie temperature. Simulated magnetization above the Curie temperature scales with cluster size as predicted by models assuming short-range magnetic ordering. Analytical approximations to the magnetization as a function of temperature and size are proposed.

I. INTRODUCTION

At the nanoscale, finite-size effects can strongly influence the magnetic properties of materials [1]. Fe layers deposited on W substrates (typically on the order of few hundreds of Fe atoms) are a prototypical example of those effects [2]. Numerical and experimental studies have extensively demonstrated the impact of the size, dimension, and number of Fe monolayers on their magnetic properties, including ordering temperature (Curie or Néel), magnetic susceptibility, or magnon dispersion relations [3–5]. In the field of magnetic nanoclusters, large departures from the corresponding bulk magnetic properties have also been observed. For example, hysteresis loop, coercive field, ordering temperature, or spontaneous magnetization, have been shown to drastically depend on the size of iron oxide nanoparticles (NPs) [6–8].

Understanding magnetism at the nanoscale is important since the computed or measured magnetic properties can be used to parametrize micromagnetic models, which are extremely valuable to simulate technological applications [9]. This is the case, for example, even in the most basic Stoner-Wohlfarth (SW) model [10], which represents the coercivity

and switching field of a magnetic single-domain NP. In its simplest form, the SW model depends on the total magnetization and anisotropy energy of the particle. It is therefore of fundamental importance to develop accurate numerical tools evaluating how the cluster magnetization is affected by temperature and particle size. Electronic *first-principles* calculations are certainly extremely valuable to obtain better insight at localized effects and to derive magnetic interaction parameters [11]. However, the involved computational costs and their poor scalability makes them unpractical for simulating NPs in the size range of technological interest, as they are typically limited to systems up to a few hundreds of atoms [12,13]. Consequently, developing reliable novel approaches is crucial for the progress in this field.

Leveraging an adiabatic atomistic spin approximation [14], atomistic spin dynamics (ASD) is a widely used classical spin-lattice methodology allowing us to model complex nanoscale systems [15–18]. Magnetic trajectories are simulated on a potential energy surface generated by a magnetic Hamiltonian usually parametrized from *first-principles* calculations [19]. Assuming fixed atomic positions, ASD simulations do not account for magnon-phonon interactions. Former studies have displayed the importance of those interactions on the description of materials properties such as magnon lifetime, phononic thermal conductivity, magnetic switching or critical

*gonzalodossantos@gmail.com

temperature [20–22]. Spin dynamics (SD) can also be used as a coarse grained approach, to compute the time evolution of blocks of the systems having many atoms with some effective magnetization. This allows the simulation of micron-sized systems that are of technological relevance [23–26]. ASD has been recently applied to Fe oxide NPs, using a triangular lattice [27].

A study accounting for the magnon-phonon interactions in molecular dynamics (MD) simulations has been performed by Dudarev and Derlet. Using a combination of the Stoner and the Ginzburg-Landau models, they developed a "magnetic" potential for α iron to take into account some effects of magnetism, including the energetics of point defects [28,29]. Later, a numerical methodology coupling MD and ASD by explicitly treating atomic and spin degrees of freedom as well as their coupling through a magnetoelastic Hamiltonian was presented by Ma *et al.* [30]. Recently, a large number of investigations have been carried out applying MD coupled to spin dynamics simulations (MD-SD) to explain experiments of magnetic instability [31], demagnetization, impact of temperature on magnetomechanical properties, and phase transitions [21,32]. This includes the development of a new software for the implementation of the model, SPILADY [33]. Perera *et al.* carried out studies of magnetic Fe using MD-SD [34], including spin-orbit coupling effects [35]. Other recent studies incorporate additional exchange parameters obtained from *ab initio* methods [36].

In this paper, SD coupled to classical MD simulations [37] is used to incorporate thermal spin and mechanical effects which are difficult to include in ASD simulations. This method is applied to Fe nanoclusters to obtain magnetization versus size and temperature, subsequently comparing those results to semianalytical models.

The paper is organized as follows. In Sec. II, the simulation framework employed is presented, as well as the details of the calculations. In Sec. III, two semianalytical models are introduced to qualitatively analyze numerical simulations. The results are presented and discussed in Sec. IV. Finally, the main conclusions are drawn in Sec. V.

II. METHODS

A. Theoretical framework

In this paper, we perform MD-SD, where the spin degrees of freedom are coupled to the lattice degrees of freedom. For this purpose, we run our simulations under the SPIN package recently added to the software LAMMPS [37]. Under this framework, one is able to introduce magnetic effects in a classical MD simulation through a generalized Hamiltonian:

$$\mathcal{H} = \sum_{i=1}^{N} \frac{|\boldsymbol{p}_i|^2}{2m_i} + \sum_{i,j,i \neq j}^{N} V(r_{ij}) + \mathcal{H}_{\text{mag}}. \quad (1)$$

The first term is the kinetic energy of the atoms and the second term is a classical interatomic potential describing the mechanical interactions between the atoms. The last term is a magnetic Hamiltonian, which can contain several terms, accounting for spin-spin exchange interactions, magnetic anisotropy (cubic, uniaxial), Zeeman, dipolar, Dzyaloshinskii-Moriya, and magnetoelectric interactions. In this paper, we

will consider isolated Fe NPs, with no interaction with external magnetic fields. The simplified magnetic Hamiltonian used in the present work is given by

$$\mathcal{H}_{\text{mag}} = -\sum_{i,j,i \neq j}^{N} J(r_{ij})\boldsymbol{s}_i \cdot \boldsymbol{s}_j + \mathcal{H}_{\text{cubic}}. \quad (2)$$

The first term is a Heisenberg Hamiltonian accounting for spin-spin interactions, where $\boldsymbol{s}_i$ is the normalized spin vector of spin i and $J(r_{ij})$ is the Heisenberg magnetic coupling exchange constant, which depends on the distance r_{ij} between atoms i and j. The second term accounts for cubic magnetic anisotropy and is given by

$$\mathcal{H}_{\text{cubic}} = \sum_{i=1}^{N} K_1[(\boldsymbol{s}_i \cdot \boldsymbol{n}_1)^2(\boldsymbol{s}_i \cdot \boldsymbol{n}_2)^2 + (\boldsymbol{s}_i \cdot \boldsymbol{n}_2)^2(\boldsymbol{s}_i \cdot \boldsymbol{n}_3)^2$$
$$+ (\boldsymbol{s}_i \cdot \boldsymbol{n}_1)^2(\boldsymbol{s}_i \cdot \boldsymbol{n}_3)^2] + K_2(\boldsymbol{s}_i \cdot \boldsymbol{n}_1)^2(\boldsymbol{s}_i \cdot \boldsymbol{n}_3)^2(\boldsymbol{s}_i \cdot \boldsymbol{n}_3)^2, \quad (3)$$

where K_1 and K_2 are the intensity coefficients and $\boldsymbol{n}_1$, $\boldsymbol{n}_2$, and $\boldsymbol{n}_3$ are unitary vectors along the three anisotropic directions of the material. For bcc iron $\boldsymbol{n}_1 = (100)$, $\boldsymbol{n}_2 = (010)$, and $\boldsymbol{n}_3 = (001)$. The anisotropy term given by Eq. (3) applies a precession torque on each magnetic spin.

The central aspect of this simulation scheme is the addition of a classical spin vector $\boldsymbol{s}_i$ to each atom i. This enables magnetic degrees of freedom to be explicitly treated and added to the atomic degrees of freedom, momentum $\boldsymbol{p}_i$, and position $\boldsymbol{r}_i$. The equations of motion (EOM) can be derived from the Hamiltonian of Eq. (1):

$$\frac{d\boldsymbol{r}_i}{dt} = \frac{\boldsymbol{p}_i}{m_i}, \quad (4)$$

$$\frac{d\boldsymbol{p}_i}{dt} = \sum_{i,j,i \neq j}^{N} \left[\frac{dV(r_{ij})}{dr_{ij}} + \frac{dJ(r_{ij})}{dr_{ij}} \boldsymbol{s}_i \cdot \boldsymbol{s}_j \right] \boldsymbol{e}_i, \quad (5)$$

$$\frac{d\boldsymbol{s}_i}{dt} = \boldsymbol{w}_i \times \boldsymbol{s}_i, \quad (6)$$

where $\boldsymbol{e}_i$ is a unit vector along the direction of the vector $\boldsymbol{r}_{ij}$ and $\boldsymbol{w}_i$ is the analog of a spin force applied to spin i, defined as

$$\boldsymbol{w}_i = -\frac{1}{\hbar} \frac{\partial \mathcal{H}_{\text{mag}}}{\partial \boldsymbol{s}_i}. \quad (7)$$

The distance dependence of the exchange constant $J(r_{ij})$ on the first term of Eq. (2) is a key aspect of the model since it mediates the spin and lattice coupling. Furthermore, $J(r_{ij})$ is modeled by a function based on the Bethe-Slater curve [38,39], parameterized using three coefficients that must be fitted to *ab initio* calculations:

$$J(r_{ij}) = 4\alpha \left(\frac{r_{ij}}{\delta}\right)^2 \left[1 - \gamma \left(\frac{r_{ij}}{\delta}\right)^2\right] e^{-\left(\frac{r_{ij}}{\delta}\right)^2} \Theta(R_c - r_{ij}), \quad (8)$$

where $\Theta(R_c - r_{ij})$ is the Heaviside step function and R_c is the cutoff distance. In the present paper, we have used the parametrization for bcc iron described in previous works [20,37] from *ab initio* calculations reported by Pajda *et al.* [40]. Specifically, the values of the fitting parameters are $\alpha = 25.498\,\text{meV}$, $\gamma = 0.281$, $\delta = 0.1999\,\text{nm}$, and exchange interaction cutoff distance $R_c = 0.34\,\text{nm}$. The same $J(r_{ij})$ applies to all atoms in the NP. Notice that there is no general

agreement about the exact value of the coupling-exchange constant for different interatomic distances for bcc Fe. In fact, the reported values of $J(r_{ij})$ from *ab initio* calculations found in the literature show large discrepancies [40–42].

Temperature in other simulation schemes, such as micro-magnetic simulations, is not uniquely defined and has to be rescaled to compare with experiments [24]. In the simulations presented here, lattice and magnetic temperatures have a clear definition. The equilibrium lattice temperature is related to the kinetic temperature of the atoms and is defined as in classical MD simulations,

$$T_L = \frac{2}{3Nk_BT} \sum_{i=1}^{N} \frac{|\boldsymbol{p}_i|^2}{2m_i}, \qquad (9)$$

where k_B is the Boltzmann constant. Following the approach of Nurdin and Schotte [43], the temperature of the spin system is defined as follows:

$$T_S = \frac{\hbar}{2k_BT} \frac{\sum_{i=1}^{N} |\boldsymbol{s}_i \times \boldsymbol{w}_i|^2}{\sum_{i=1}^{N} \boldsymbol{s}_i \cdot \boldsymbol{w}_i}. \qquad (10)$$

In addition, in these spin-lattice simulations, the effect of temperature in lattice expansion is more realistic (due to the spin-lattice coupling) than in some previous approaches, which consider, for example, an homogeneous linear thermal expansion of the lattice with fixed atoms [44]. To thermalize the system and maintain a constant temperature, both the lattice and spin subsystems can be connected (separately) to a thermal bath. This connection is performed following the Langevin approach [14,45]. For the SD, this connection intro-duces a random torque and Eq. (6) is replaced by a stochastic Landau-Lifshitz-Gilbert equation, while for the lattice subsys-tem a damping term and a random force are added to Eq. (5). This yields the following EOM:

$$\frac{d\boldsymbol{r}_i}{dt} = \frac{\boldsymbol{p}_i}{m_i}, \qquad (11)$$

$$\frac{d\boldsymbol{p}_i}{dt} = \sum_{i,j,i\neq j}^{N} \left[\frac{dV(r_{ij})}{dr_{ij}} + \frac{dJ(r_{ij})}{dr_{ij}} \boldsymbol{s}_i \cdot \boldsymbol{s}_j \right] \boldsymbol{e}_i$$
$$- \frac{\gamma_L}{m_i} \boldsymbol{p}_i + \boldsymbol{f}(t), \qquad (12)$$

$$\frac{d\boldsymbol{s}_i}{dt} = \frac{1}{1+\lambda^2} [(\boldsymbol{w}_i + \boldsymbol{\eta}(t)) \times \boldsymbol{s}_i + \lambda \boldsymbol{s}_i \times (\boldsymbol{w}_i \times \boldsymbol{s}_i)], \qquad (13)$$

where λ and λ_L are damping parameters for the spin and lat-tice subsystems, respectively. In addition, the random vector $\boldsymbol{\eta}(t)$ and the random fluctuating force $\boldsymbol{f}(t)$ are drawn from a Gaussian probability law with $\langle \boldsymbol{\eta}(t) \rangle = \langle \boldsymbol{f}(t) \rangle = 0$. For extra details on thermostats and the properties of $\boldsymbol{\eta}(t)$ and $\boldsymbol{f}(t)$, see Ref. [37]. The interaction between atoms is modeled us-ing an embedded atom model (EAM) interatomic potential [46] which describes reasonably well several Fe properties, including the thermal expansion, phonon dispersion curves, mean-square displacements, and surface relaxations. The in-teratomic cutoff distance for this potential was set to 0.35 nm.

The simulations are performed using classical atomic dynamics and classical SD, without considering any quantum-mechanical effects. This is in line with the adiabatic approx-imation. However, the behavior at cryogenic temperatures
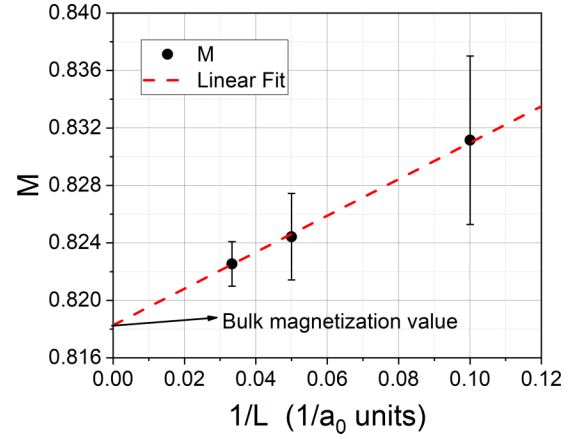

FIG. 1. Finite-size scaling for bulk magnetization simulations, using periodic boundary conditions. The data correspond to simu-lations run at 300 K and error bars show standard deviation resulting from averaging magnetization over the final 0.5 ns.

might not be well described. Moreover, other effects result-ing from electron-phonon and electron-spin coupling are not included. There are studies which include electrons within a "classical" two-temperature model approach for electrons and atoms, leading to a three-temperature model when spins are also included [33].

The SD is calculated using a Landau-Lifshitz-Gilbert approach [14], integrated with a Suzuki-Trotter integrator. Details can be found in Tranchida *et al.* [37].

B. Simulation details

Body centered cubic (bcc) iron NPs are simulated ranging their diameter and temperature from 2 to 8 nm and from 10 to 1300 K, respectively. In addition, "bulk" simulations were run and used as a reference to address the finite-size effects of the NPs. In these cases, we have modeled cubic simulation boxes with linear sizes of $10\,a_0$, $20\,a_0$, and $30\,a_0$ (with $a_0 = 2.8665$ Å the bcc Fe lattice parameter) containing 2000, 16 000, and 54 000 atoms, respectively, and considering periodic boundary conditions in the three directions.

The magnetization values for the bulk systems were ob-tained from linear finite-size scaling analysis. As shown in Fig. 1, the magnetization values for the systems with $L = 10$, 20, and 30 are plotted as a function of $1/L$, and then the bulk magnetization is determined as the intercept of a linear fit for those points.

All systems were simulated without external magnetic field, and considering cubic magnetic anisotropy along the three main axes of the bcc lattice (details of how the anisotropy is included in the simulations are given in Ref. [37]). The anisotropy constants were set to $K_1 = 3.5\,\mu\text{eV/atom}$ and $K_2 = 0.36\,\mu\text{eV/atom}$ [47]. It has been argued that anisotropy values vary near the surface of NPs due to the reduction of coordination [48,49]. Nevertheless, as shown by Ellis and Chantrell [50], for example, the overall effect in FePt NPs of 4.632 nm and 2.316 nm is a change of about 10% in the anisotropy constant. In this paper, the anysotropy constant is assumed to be the same for all NPs,
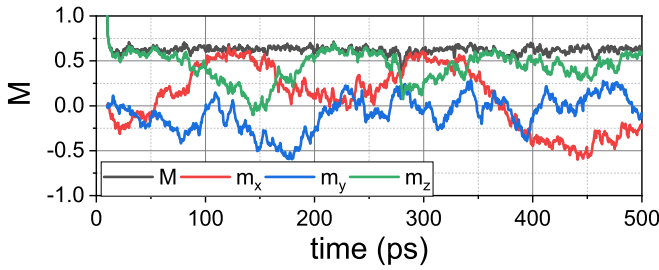
FIG. 2. Time dependence of the components m_x, m_y, m_z, of the magnetization along the x, y, and z axes and the total magnetization M during a typical simulation. The results correspond to simulations of a 2-nm-wide sphere at 400 K.
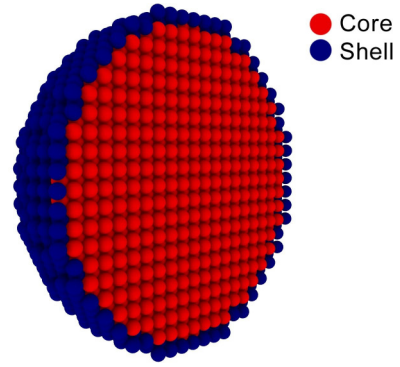

FIG. 3. Snapshot of one half of a 6-nm diameter Fe NP, obtained with software OVITO [52], inscribed in a cubic region with periodic boundary conditions. The shell and core regions are indicated by the colors, where each small sphere represents an atom.

244 despite surface proportion being clearly different for the sizes
245 studied here.
246   Initially, all atomic spins were oriented along the z axis
247 ([001] direction). This initial configuration was chosen since
248 the magnetization reaches an equilibrium value faster than
249 when the spins start from a random configuration (see Fig.
250 S1 in the Supplemental Material [51]).
251   All simulations span more than 0.5 ns, using a time step of
252 1.0 fs. All samples were initially thermalized to equilibrium
253 using a Langevin thermostat applied to the lattice and another
254 thermostat applied to the spins to ensure fast thermal equilib-
255 rium. In all cases, we used a damping factor of $\lambda_L = 1.0$ for
256 the lattice thermostat and a transverse damping $\lambda_s = 0.1$ for
257 the spin system. Before the thermostat was applied, atomic
258 velocities were set so as to obtain an initial temperature of
259 300 K (or 10 K in the cases of the simulations with T <
260 300 K). Applying the thermostat, thermal equilibrium was
261 reached in all cases in a time between 2 ps and 10 ps with
262 some fluctuations around the set temperature. Similarly, the
263 resulting magnetization quickly reaches a stable value and
264 remains stable during the simulation although its components
265 may fluctuate, as shown in Fig. 2.
266   Once the simulation results were obtained, we conducted
267 post-processing analyses using the free software OVITO [52].
268 In particular, we employed the coordination analysis tool to
269 distinguish between atoms in the outer layer of the sphere
270 (shell or surface) and the inner ones (core) to obtain the mag-
271 netization curves of these two different regions. In all cases,
272 a single layer of atoms was selected within the surface group,
273 as shown in Fig. 3. Details of the number of atoms contained
274 in each NP and the ones belonging to the surface and the core
275 regions are presented in Table I.

Total magnetization averages were computed over the last 276
300 000 steps of the simulation. To minimize computational 277
cost, core, and shell magnetization (M_c and M_s, respectively) 278
results were obtained averaging over the last 100 ps of the 279
simulation. 280

III. MEAN-FIELD ISING MODELS

Coupled MD-spin simulations are an advanced modeling 282
tool that has never been applied to magnetic NPs. It is there- 283
fore useful to probe our results by comparing them to simpler 284
and more commonly used models. In this section, two variants 285
of the mean-field Ising model have been applied to NPs to 286
perform that comparison. 287

A. Spin model including surface effects

Our results can be compared with a theoretical model that 289
includes surface effects on the magnetization. This model, 290
originally proposed by Mills [53], is known as semi-infinite 291
Ising model with a free surface, i.e., basically a mean-field 292
Ising model of a ferromagnet with a free surface. It is assumed 293
that the spins are arranged in a lattice (bcc in this case) and 294
that the spins in all lattice sites are given by $S_i = \pm 1$ where 295
$S_i = +1$ means that spin i is pointing along the positive z 296
direction and $S_i = -1$ means that spin i is pointing in the op- 297
posite direction. In this model, the exchange coupling constant 298
J is the same for all nearest-neighbor (NN) pairs, except for 299
the case of pairs at the surface of the ferromagnet where it is 300
denoted by J_s. A layered structure is then obtained with the 301
Hamiltonian being given by 302

$$\mathcal{H} = -J \sum_{\langle i,j \rangle \notin S}^{N} \boldsymbol{\mu}_i \cdot \boldsymbol{\mu}_j - J_s \sum_{\langle i,j \rangle \in S}^{N} \boldsymbol{\mu}_i \cdot \boldsymbol{\mu}_j. \quad (14)$$

Following the mean-field approach, the magnetization for 303
the surface m_s and for each successive layer $m_1, m_2, \ldots m_n$, 304
are given by 305

$$m_s = \langle \mu_{i \in S} \rangle = \tanh(4K_S m_S + K m_1), \quad (15)$$

$$m_1 = \langle \mu_{i \in 1} \rangle = \tanh(4K m_1 + K m_S + K m_2), \quad (16)$$

TABLE I. Total number of atoms, surface atoms, core atoms, and percentage of surface and core atoms for each studied Fe nanocluster.

Diameter	No. of atoms	Surface atoms	Core atoms	% surface	% core
2 nm	339	177	162	52.21	47.79
3 nm	1243	528	715	42.48	57.52
4 nm	2741	808	1933	29.48	70.52
5 nm	5601	1480	4121	26.42	73.58
6 nm	9577	2054	7523	21.45	78.55
8 nm	22659	3695	18 964	16.31	83.69

$$m_n = \langle \mu_{i \in n} \rangle = \tanh(4Km_n + Km_{n-1} + Km_{n+1}), \quad (17)$$

where $K_s = \beta J_s$ and $K = \beta J$ with $\beta = 1/k_B T$ and k_B is the Boltzmann constant. It is important to notice that K and K_s are not related to the anisotropy constants K_1 and K_2 described previously. In this paper, we have adopted a two-layer approximation, meaning that we have considered that the system's magnetization is unaltered after the first layer (the one after the surface), $m_1 = m_2 \cdots = m_n = m_{\text{bulk}}$. Therefore, m_1 represents the cluster core magnetization and, in addition, we have set $J_s = J$. In this way, the summation on the first term of the right-hand side of the Hamiltonian [Eq. 14], runs over the eight first neighbors (core) and the one on the second term runs over four first neighbors [(100)-like surface]. Related electronic models have been used to obtain the magnetization of Fe thin films [44].

B. Spin model including finite-size effects

A previous theoretical model developed in Ref. [54] is summarized below. The model is based on the mean-field approximation for the Ising model, adapted to the statistics of few-particle systems. The mean-field approach is well known and does not need explanation. However, if a few-particle system is analyzed, we should be careful with the approximations that are used when obtaining the fundamental equations in the microcanonical formalism [55]. In particular, the Stirling approximation ($\ln x! \approx x \ln x - x$) cannot be applied, and the factorial must be written in terms of the Gamma function: $\Gamma(x) = (x + 1)!$. This implies working with the derivative of this function, known as the digamma function:

$$\psi^{(0)}(x) = \frac{d\Gamma}{dx}. \quad (18)$$

Taking this into account, a self-consistent equation for the magnetization M is found. If there are N atoms in the system and the coordination number between them is z, the magnetization is given by the solution of the equation

$$M = \frac{k_B T}{zJ} \left\{ \psi^{(0)} \left[\frac{N}{2}(1 + M) + 1 \right] - \psi^{(0)} \left[\frac{N}{2}(1 - M) + 1 \right] \right\}. \quad (19)$$

Naturally, this simple model does not allow us to make precise quantitative predictions due to the coarseness of the mean-field approach. However, one could expect to obtain a reasonable qualitative comparison with the results of the simulations. Equation (19) has to be solved numerically for the conditions in each simulation.

IV. RESULTS AND DISCUSSION

A. Simulation results

Typical initial atomic and spin configurations and its evolution after 500 ps of simulation can be seen in Figs. 4 and 5 for different NP sizes and temperatures. For more insight about the individual atomic spins dynamics, the reader is referred to movies SM1 and SM2 in the Supplemental Material [51], where evolution of simulations are shown for a group of spins
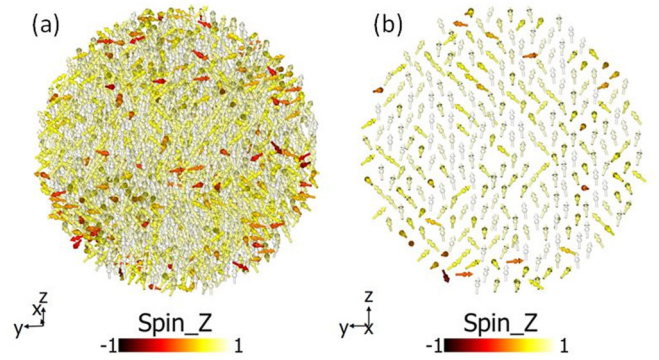

FIG. 4. Snapshots of a typical simulation of a NP with a diameter of 6 nm. In (a), the atomic spins are displayed as arrows, with color indicating magnitude of m_z at 600 K. (b) Same as (a) for thin slab at the center of the nanoparticle. The initial condition of the simulations was $m_z = 1$, i.e., all spins pointing along the positive z axis. See also the movies SM1 and SM2 in the Supplemental Material [51].

belonging to a slab at the center of the sphere (SM1) and also for the spins from the surface of the NP (SM2).

The temperature dependence of the total magnetization is shown in Fig. 6 for NPs of 2, 4, and 8 nm in diameter, along with the bulk system. Results for all simulated clusters are not included in this graph to avoid cluttering; a graph with the complete set of the simulated NPs appears in Fig. S2 of the Supplemental Material [51]. Figure 6 indicates that the bulk Curie temperature, T_C, in our simulations is around 650 K, lower than the 1040 K in experiments, and this difference
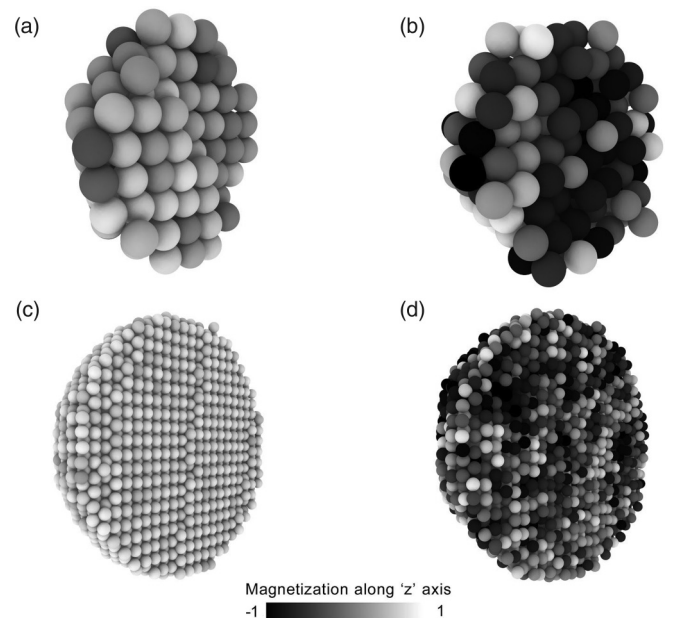

FIG. 5. Snapshots of simulations showing the z-component m_z of the atomic magnetization for nanoparticles having (a) 2 nm and 300 K, (b) 2 nm and 1200 K, (c) 6 nm and 300 K, and (d) 6 nm and 1200 K. The small spheres represent atoms. White indicates that the spins point along the positive z axis, while black indicates that m_z points along the negative z axis. The z axis is vertical with the positive direction pointing upward in the figures.
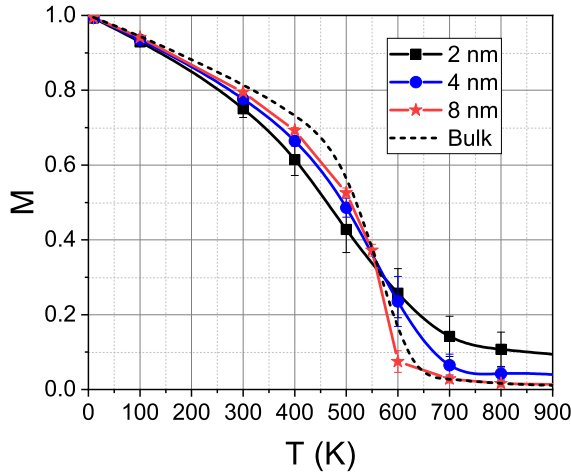
FIG. 6. Total normalized magnetization as a function of temperature for different NPs compared to the bulk values.
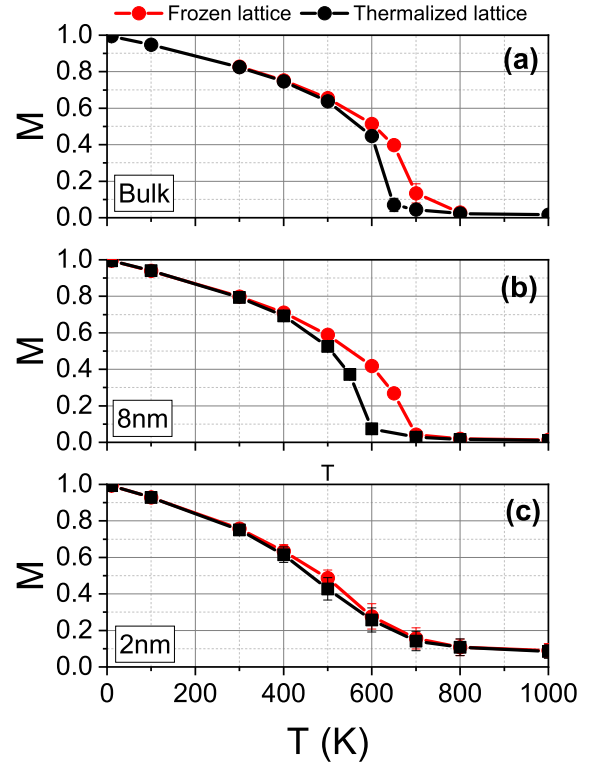

FIG. 7. Temperature dependence of the magnetization $M(T)$ as obtained using MD-SD, for (a) Fe bulk, nanoparticle diameters (b) 8 nm, and (c) 2 nm. The results for thermalized and frozen translational degrees of freedom are compared. Bulk results correspond to cubic simulation boxes with $20\,a_0$ sides.

is discussed later. From Fig. 6, there are indications of an increase of T_C with decreasing cluster size, reaching around $T_C \sim 800$ K for a 2-nm cluster with $\sim$500 atoms.

At the low-temperature regime, as the size of the Fe nanoclusters is reduced, the magnetization takes lower values than the bulk ones for all sizes. The difference is larger as the temperature is increased up to about 550–600 K. This is the expected behavior since the surface contribution to the total magnetization is more important in smaller NPs due to the larger surface/bulk proportion (see Table I). When the temperature is raised to about $T \approx 500$ K, the surface magnetization decreases faster than the core contribution since the spins on the outer layer, having smaller local coordination number, are disordered more easily (see Fig. 11). For temperatures higher than 500 K, the bulk magnetization is the one that decreases faster, i.e., changing to the opposite behavior. This is displayed by the interception of the curves around T $\approx$ 550 K in Fig. 6. A similar crossover has been also observed in other studies of magnetic NPs [50,56].

It is interesting to compare our results with those of simulations in which the atoms are static. In Fig. 7, we have compared the magnetization curves with the ones corresponding to NPs with fixed atomic positions. At low temperatures, below 400 K, there is no significant difference. Our results for bulk Fe are consistent with other simulations which found only a small decrease of the critical temperature with the inclusion of a thermalized, moving lattice [36,57]. For the 2-nm case, the moving atoms lead to a minor decrease in magnetization, since the NP is already quite disordered, from a magnetic point of view, at temperatures where the fluctuations of the interatomic distances become important due to the large fraction of surface atoms (see Table I). For the 8-nm case, magnetization goes to zero at lower temperatures for the moving atoms, as expected from the bulk simulations. At 600 K, near the critical temperature, the mean value of the NN distances changes less than 1% with respect to the one for the frozen lattice. As a result, the value of $J(r_{ij})$ averaged over the distribution of NN atomic distances at 600 K is only slightly different than the value $J(r_{NN})$ for fixed atoms, changing less than $\sim$3%. Therefore, neither a lattice expansion nor

a fluctuating mean value for J can explain the decrease in magnetization found in our simulations for a moving lattice. This is a clear indication that the coupling between lattice and spins play a significant role for not-too-small Fe particles near T_C. Calculation of time and spatial correlation functions might help understanding this in detail.

Complementary insight is obtained by comparing our results with simulations for static spins in a regular lattice [58]. Let us assume only NN interactions and $J = 15$ meV, similar to the value in our simulations for distances between first and second neighbors. The Ising model in 3D gives $T_C = zJ/k_B$ for the mean-field approximation, where z is the coordination number (8 for bcc) resulting in $T_C = 1393$ K. However, Bethe's solution gives $T_C \approx 2J/k_B \ln(z/(z-2)) \approx 1200$ K. The classical Heisenberg model gives $T_C \approx 4zJ/3k_B = 1857$ K, using the mean-field approximation. Using a high-temperature expansion, this changes to $(105/96)(z-1)J/k_B = 1333$ K [58]. As expected, the mean-field approximation overestimates the Curie temperature compared to the exact analytical models or to numerical solutions.

Our NPs magnetization results are consistent, and show really good agreement, with the experimental magnetization curves for Fe nanoclusters reported by Billas *et al.* [59], Fig. 8(a), where it can be seen that both the shape of the curves and the estimated Curie temperature for the iron nanoclusters are well reproduced. To compare with experimental results, we have assumed a constant local magnetic moment of $2.2\,\mu_B$.
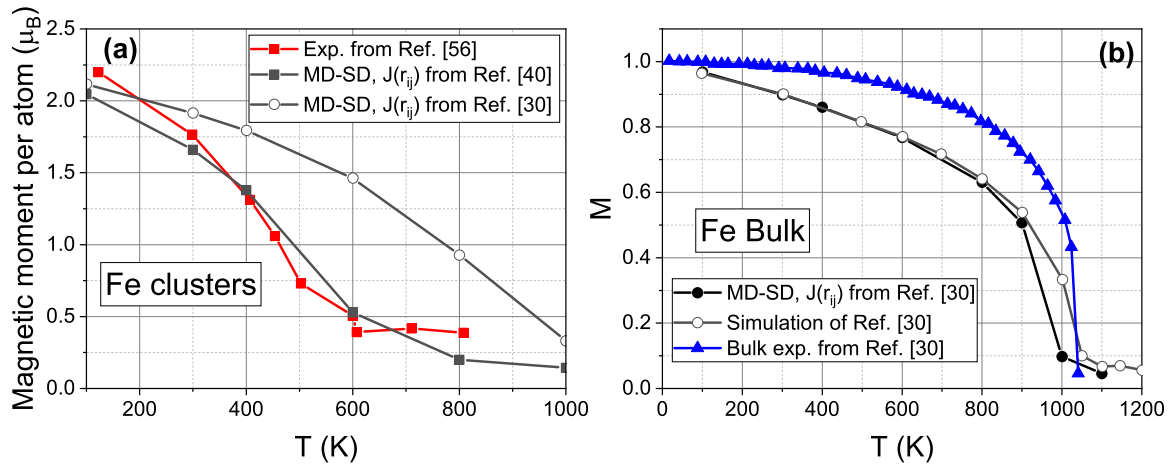
FIG. 8. (a) Experimental results for a Fe nanocluster of about 500–600 atoms as reported by Billas *et al.* [59] compared to the results of our simulations of a Fe NP composed of 533 atoms using two different exchange functions $J(r_{ij})$. The exchange function $J(r_{ij})$ fitted from the calculations of Pajda *et al.* [40] is the one used in this work and it reproduce quite closely the experimental results. The open circles correspond to simulation results using the exchange function proposed by Ma *et al.* [30]. (b) Magnetization of a Fe Bulk system (cell size $20 \times 20 \times 20 a_0^3$) as obtained using the exchange function proposed by Ma *et al.* [30] (full circles). Bulk experimental data (triangles) and the results reported by Ma *et al.* (open circles) are also shown for the sake of comparison.

While our simulation results match with experiments for small clusters, our bulk simulations yield an estimated Curie temperature around $T_C \approx 650$ K, far below the experimental value of 1043 K. The main reason for this discrepancy is the exchange coupling function used in this paper. When $J(r_{ij})$ is replaced, for example, by the one used by Ma *et al.* [30] (note the large discrepancies found in the literature for $J(r)$ reported in Fig. 1 of Ref. [30]), our simulations show similar results regarding the experimental Fe Curie temperature, as the results reported in that paper [Fig. 8(b)]. Should one use those parameters for small clusters, one obtains an overestimation of the cluster T_C. Hypothetically, this is an indication of an important increase of the effective exchange function $J(r_{ij})$ as the size of the NPs increase. It also reflects the challenge of modeling broad size ranges in the size-dependent effective interaction parameters.

Some recent SD simulations which incorporate finite-temperature effects obtain a lower Curie temperature, T_C, than experimental values [36,60]. It is known that SD simulations tend to smooth the ferromagnetic-paramagnetic transition near the Curie temperature due to the intrinsic coarse-graining of the numerical scheme and since quantum effects are not taken into account [20]. Nevertheless, adding a quantum mechanical treatment does not guarantee a correct determination of T_C [61]. The discrepancy between T_C obtained in our simulations and the experimental one could also be partly related to the fact that our magnetic exchange function $J(r_{ij})$ is not temperature nor size sensitive. In fact, in this framework, it is not possible to take into account any temperature-dependence changes in the electronic structure from which $J(r_{ij})$ is obtained. Modeling an exchange parameter that is function of T is expected to lead to a more precise estimation of T_C [20,62,63]. In addition, including system-size variations of $J(r_{ij})$ might help reproducing the changes in T_C which can be derived from Fe cluster experiments [59].

Figure 9 displays the size dependence of the total magnetization $M(T)$ which is plotted as a function of the inverse

diameter for representative temperatures T. This allows us to show the bulk magnetization values corresponding to $1/d = 0$. At low temperatures, the calculated size dependence is almost negligible. This trend contrasts with the well-known enhancement of the average ground-state magnetization in Fe clusters and surfaces, which can be qualitatively explained from an electronic perspective as a consequence of $3d$-band narrowing [64]. The effect could be easily incorporated in our simulation by taking into account the size dependence of
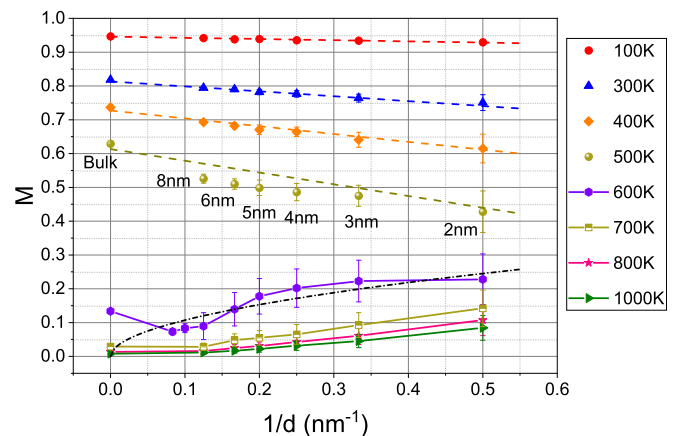

FIG. 9. Size dependence of the total magnetization at different representative temperatures. The normalized magnetization is plotted as a function of the particle inverse diameter ($1/d$). Symbols and full curves correspond to the simulation results, whereas the dashed lines represent the fitted curves. The error bars indicate the standard deviation of the data that are taken into account in the average over the last 0.3 ns. For the fitted curves, the function is $M = a(1 - b^T)(1/d) + (\frac{T-T_C}{T})^{1/3}$ where $a = 0.1$, $b = 1.003$, and $T_C = 650$ K. The black dash-dotted line corresponds to $M = 0.35(1/d)^{0.514}$ and is related to the magnetization scaling behavior near the critical temperature in the 3D Heisenberg model as detailed in the text.

the local magnetic moment $\mu_i = |\langle s_i \rangle|$. As the temperature increases, so does the influence of the NP size on the total magnetization. These results are in good agreement with those reported by Iglesias and Labarta [7], who studied the size effects on maghemite NPs via Monte Carlo simulations.

It is notable that Fig. 9 clearly shows two different regimes: low ($T < 600$ K) and high ($T > 600$ K) temperatures, separated by the 600 K curve. For temperatures below 600 K, we find that the magnetization behavior is almost linear with the inverse diameter, showing higher values for larger NPs. This trend is expected, as adding more magnetic atoms to the particle stabilizes a stronger ferromagnetism, and thus increases the resilience of the total magnetization to thermal disorder. In addition, this linear size dependence is stronger when the temperature is increased. To further analyze these results, we have proposed a functional with only two free parameters for the magnetization as a function of temperature and cluster size. This approximation manages to reproduce the size dependence of the magnetization very well for temperatures below 600 K, as can be seen from the dashed lines in Fig. 9. The corresponding function is

$$M(T, d) = a(1 - b^T)\frac{1}{d} + \left(\frac{T_C - T}{T_C}\right)^{1/3}, \qquad (20)$$

with $a = 0.1$, $b = 1.003$, $T_C = 650$ K, and d the NPs diameter.

For temperatures above 600 K, the linear relation between $M(T)$ and $1/d$ is reversed, although the trend remains almost linear. At higher T, larger NPs retain less magnetization than smaller ones. This qualitative change reflects the intersection of the magnetization curves in Fig. 6.

The two different regimes observed in Fig. 9 are separated from each other by the 600 K curve, where a different trend is observed. This different behavior may be due to competing effects, as the system is close to the critical temperature.

Behavior of the magnetization with varying size is governed by finite-size scaling laws. According to finite-size scaling theory [66,67], magnetization near the critical point should scale with size as $M \approx L^{(\beta/\nu)}$, where β and ν are the critical exponents related to the order parameter and correlation length, respectively. This means that the value of the magnetization for the bulk near the critical point would be lower than the simple extrapolation from a linear fit, as the one shown in Fig. 1. Magnetization near the critical temperature is expected to scale as $M(1/L)^{(\beta/\nu)} = (1/L)^{0.514}$, where $\beta/\nu = 0.514$ is the estimated value for the critical exponents of the 3D Heisenberg model [68–71]. Therefore, the bulk value should be closer to the values for finite size NPs, as also shown in that figure. In addition, the behavior of the 600 K curve for clusters is also consistent with these arguments, as shown by the dashed-dotted line in Fig. 9, corresponding to $M = 0.35(1/d)^{0.514}$.

In practice, Fig. 9 shows that even above T_c, small subclusters of atoms with similar spin orientations nucleate in the NPs as well as in the bulk cells (before rapidly dissipating). In large NPs and bulk cells, those local clusters are likely to be averaged down by the larger number of atoms, or by other local clusters with opposition magnetization. As NPs are getting smaller, fewer clusters can nucleate and thus cannot average
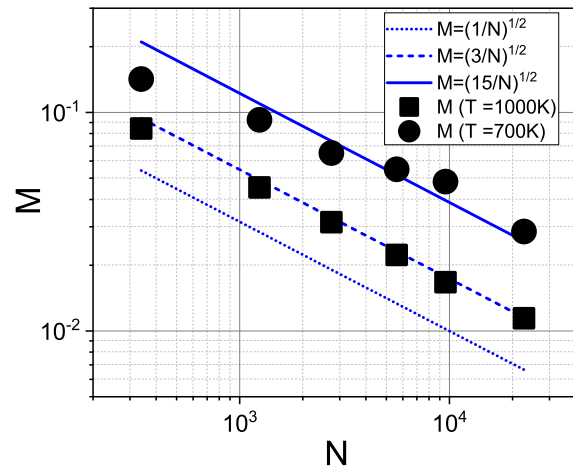

FIG. 10. Fe NP magnetization as a function of the number of atoms N in the nanoclusters (symbols) at two representative temperatures above the predicted cluster T_C, compared with different power law relations, including the one proposed in Ref. [65], for clusters with 15 atoms.

down the resulting local magnetic moments of each others. This results in the persistence of a small net magnetization at higher temperature. The trend observed above 600 K may be thus explained by the presence of spin-spin correlations above the Curie temperature. Indeed, short-range magnetic ordering (SRMO) is known to persist in the paramagnetic state of iron bulk and surfaces [72–74]. The importance of SRMO in Fe above the Curie temperature has been explicitly demonstrated in Ref. [65], where it was shown that correlated clusters with size N_{cl} for a system with N atoms led to a magnetization $M \propto (N_{cl}/N)^{1/2}$, with $N_{cl} = 15$ for Fe. This dependence is similar to the one above from finite size-scaling, and $N_{cl} = 15$ is consistent with 1st and 2nd NN shells in the bcc lattice, totalling 14 atoms, which is expected since the 2nd NN shell is only around 14% further away than the NN shell, as it is shown later in this section. Fig. 10 shows that our MD simulations near T_C, at 700 K, follow this relationship extremely well, and that for larger temperatures N_{cl} decreases significantly, due to thermal fluctuations decreasing magnetic correlation as expected. In future work, the temperature dependence of spin-spin correlation functions and related structure factors could be evaluated for different NP sizes in order to study this in detail.

The two different regimes observed in Fig. 9 may also be explained by assuming distinct core and surface magnetizations. Making this distinction, the total magnetization can be written as $M(T) = M_c(T) - [M_c(T) - M_s(T)]\frac{1}{d}$, where $M_c(T)$ and $M_s(T)$ represents, respectively, the core and shell magnetization contributions for a NP of diameter d. In this way, the total magnetization is closer to the bulk magnetization as the size of the NP increases. Consequently, if $M_s(T)$ decreases faster than $M_c(T)$ as the temperature is increased, the slope of M vs. $(1/d)$ becomes steeper, ($[M_c(T) - M_s(T)]$ becomes larger), which is the case observed in Fig. 9 until $T = 500$ K. At 600 K, for the smaller NPs ($\frac{1}{d} \geqslant 0.33$), both the interior and surface spins are disordered, that is, $M_c(T) \simeq M_s(T)$ and the curve is flatter, i.e. practically does not depend
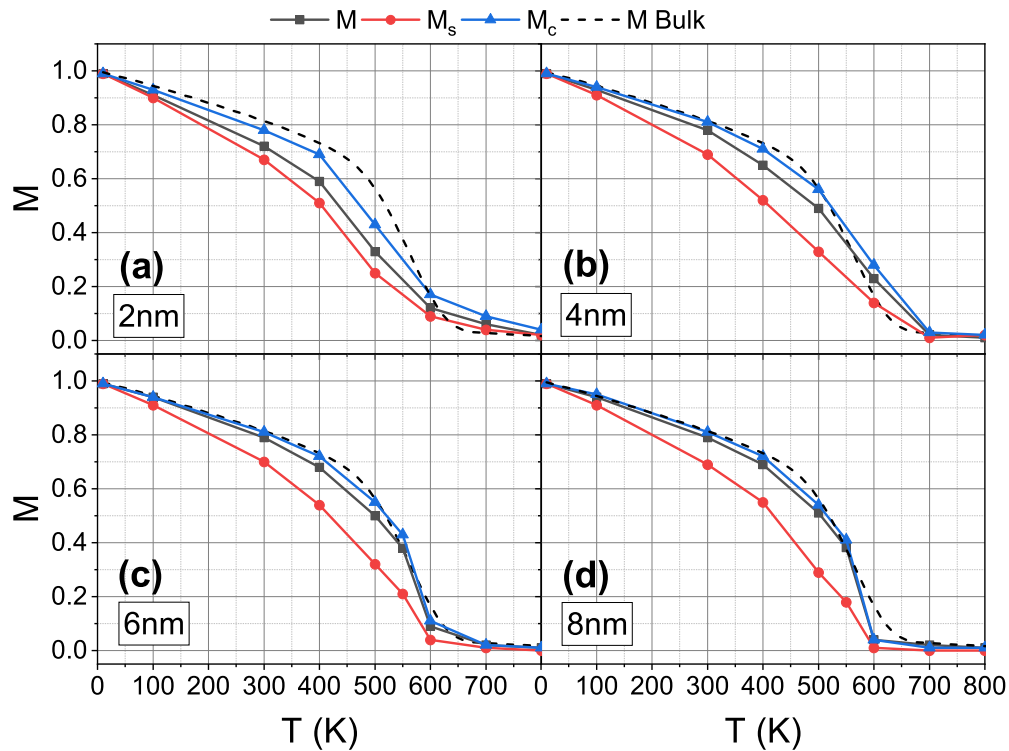
FIG. 11. Total normalized magnetization M, core magnetization M_c and shell magnetization M_s a functions of temperature for Fe NPs having different diameters. The Fe bulk magnetization is also shown.

on $1/d$. For larger nanoclusters, both shell and core spins are disordered, resulting in a small global magnetization.

Having a free surface on the NPs naturally introduces finite-size effects on the thermal behavior of the magnetization. The effects of the free surface were studied for different NPs and results are shown in Fig. 11. Surface (red dots) and core (blue triangles) contributions to the total magnetization (black squares) are plotted along with bulk magnetization results (dashed line). Surface magnetization is calculated averaging over the atoms belonging to a single-atom wide spherical shell composed of the outer layer of atoms as described in sub-section (II-B) (see Fig. 3).

The width of the surface is held constant for all spheres. The main qualitatively result is that the NPs retain less magnetization than the bulk system and this difference in magnetization increases as the particle size decreases. This is a consequence of the low coordination of the spins at the surface, together with the large surface-to-volume ratio and their contributions to the total magnetization. In this way, it is clear that for the 2nm sphere the surface contribution is as relevant as the core one. Therefore, all three curves, M, M_s and M_c, are far apart from the bulk values. As the particle diameter increases, the surface contribution to the total magnetization decreases. Thus, two main features can be seen: the total magnetization becomes increasingly similar to the core magnetization and, straightforwardly, the core magnetization approaches more and more the bulk magnetization values. This tendency of the core magnetization to approach to the bulk values is stronger at low temperatures, while near T_C there is still a clear departure from the bulk behavior. In addition, there is a temperature range where the cluster magnetization behavior and, in particular, the surface contribution

displays an approximately linear temperature dependence, as it has been previously reported by Iglesias and Labarta [7]. Furthermore, this temperature range is larger for smaller particles. In Ref. [7], it was argued that this linear behavior was related to an effective 3D–2D dimensional reduction of the surface shell, and that it has been observed in thin film systems and in simulations of rough ferromagnetic surfaces [75–79].

The surface, core and total magnetization are related by

$$M = pM_s + (1 - p)M_c, \tag{21}$$

where $p = N_s/N_T$ is the shell fraction, N_S (N_T) being shell (total) number of atoms [7]. Assuming that the shell is much thinner than the NP radius, one can arrive at the approximate expression

$$M(d) = M_c - \Delta M \frac{\Delta rS}{V} = M_c - \Delta M \frac{6\Delta r}{D}, \tag{22}$$

where S (V) are the surface (volume) of the particle, Δr is the thickness of the surface layer, D is the diameter of the spheres and $\Delta M = M_c - M_s$. Figure 12 displays a good agreement between the simple two component approximation and our simulation results. In particular, Eq. (22) manages to reproduce the intersection of the curves around T_C, a fact that is related to the surface/core proportion as discussed above.

B. Exploring possible NP premelting

The EAM potential used in the previously mentioned study yields a bulk melting temperature $T_M \simeq 2000$ K [80]. However, small clusters are expected to have much lower T_M due to the reduced surface coordination number. Indeed, in Ref. [81], a reduction of about 30% in the melting temperature of 2-nm
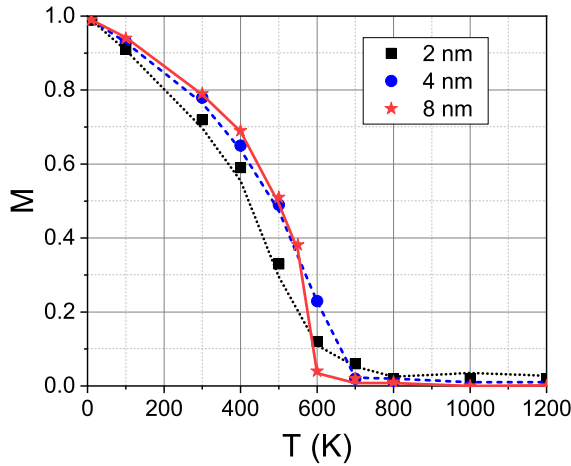
FIG. 12. Temperature dependence of the total magnetization M of Fe NPs. The results of our MD-SD simulations (symbols) are compared with the core-shell two component model described by Eq. (22) (curves).

FIG. 14. Correlation function in the core and shell regions of a 2nm Fe NP at $T = 1200\,K$.

Fe clusters has been reported. Assuming the same reduction of T_M for the EAM potential used here would give $T_M \simeq 1350\,K$. The structure and diffusivity of core and shell atoms have been analyzed at different temperatures, to evaluate possible premelting of Fe nanoclusters in the framework of our model. The pair correlation function, $g(r)$, for the whole nanocluster, is shown in Fig. 13. There are broad but well defined peaks for second- and third-NNs at high temperatures, as expected for a crystalline solid.

At 1200 K, the NN distance for bulk Fe is 0.245 nm, while for the smallest NPs this distance is closer to 0.25 nm, which correpond to a change of only 2%. The effect of large changes in neighbor distance for Fe films was evaluated by Garibay-Alonso *et al.* [44], who also observed a nearly linear decrease of the layer magnetization with temperature, as in Fig. 11. The radial distribution functions $g(r)$ shown in Fig. 14 for

$T = 600\,K$, show that there are non-negligible fluctuations on the first and second-neighbor separation distance as the size of the system is reduced. These fluctuations may result in values of $J(r_{ij})$ (see parametrization of $J(r_{ij})$ in Ref. [37]), that could drive the systems into an antiferromagnetic phase for the smallest clusters at 600 K, as it is shown in Ghosh *et al.* [82].

In Fig. 14, results are given for the interatomic correlation function $g(r)$ in the shell and core regions at a temperature near the cluster T_C. The well-defined peaks in $g(r)$ show no evidence of surface premelting at this temperature, even for the smallest NPs. To further investigate this mater, we have carried out atomic diffusivity calculations. At 600 and 1200 K, diffusivity for core atoms has a value close to zero, but for shell atoms has values of the order of $D = 4.0 \times 10^{-10} m^2/s$, as seen in Fig. 15. For reference, the bulk self-diffusion coefficients values are around $D = 1.0 \times 10^{-15} m^2/s$ for 1000 K as reported in Ref. [83]. The diffusivity for molten
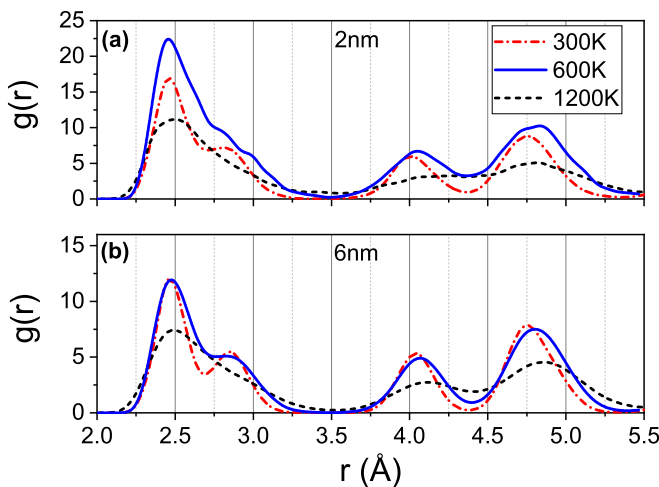

FIG. 13. Coordination analysis for spherical Fe NPs with diameters (a) $d = 2$ nm and (b) $d = 6$ nm at different temperatures. The data are taken from the last configuration of the system. They indicate lack of melting, even for the smallest considered nanocluster.
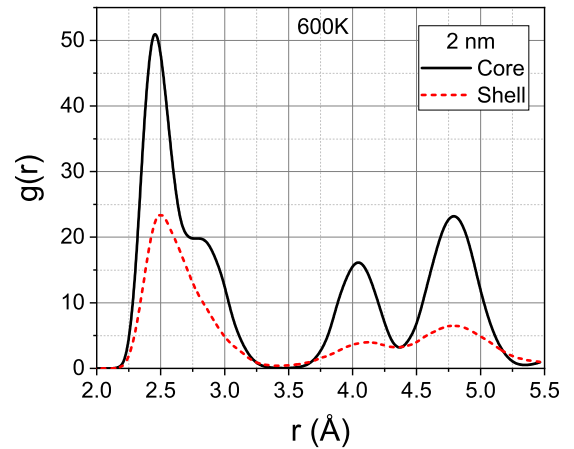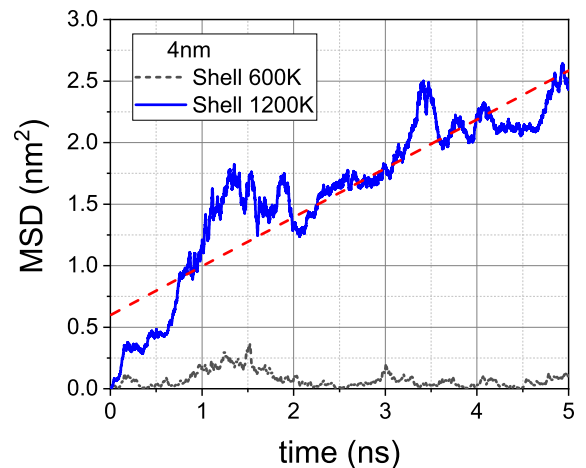

FIG. 15. Mean-square displacement of the shell atoms at 600 and 1200 K, as obtained from our simulations for a 4 nm NP. The straight dashed line represents a linear fit of the 1200 K results, giving a diffusion coefficient $D = 4.0 \times 10^{-10} m^2/s$. Note that this simulation is 10 times longer (5 ns) than those performed for the magnetization calculations.
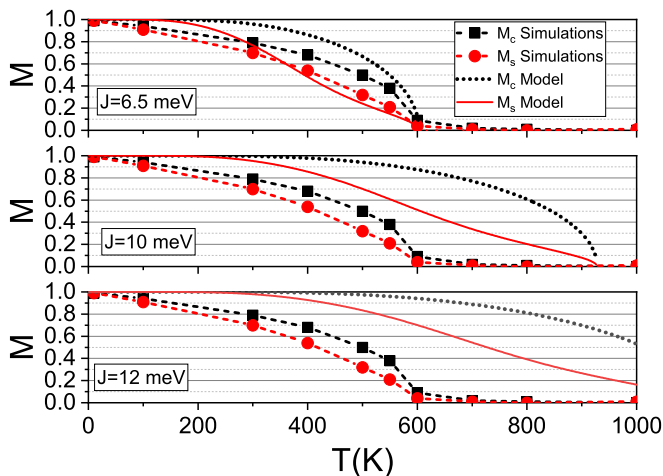
FIG. 16. Temperature dependence of the core and shell magnetizations as obtained from the semi-infinite Ising model with a free surface for different values of the exchange constant J (Sec. III A) compared with MD-SD simulations results. The curves are obtained for a Fe NP with a diameter of 6 nm.
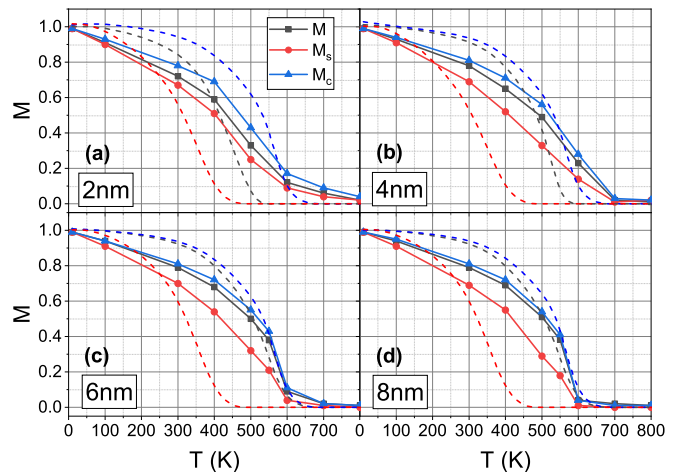

FIG. 17. Total, core and shell magnetization curves M, M_c, M_s, as obtained in the model presented in Sec. III B (dashed lines) [54] and in the present MD-SD simulations (solid line and symbols) for Fe NPs having different diameters.

Fe has been typically calculated above 1500 K. For instance, Gosh *et al.* [84] used the EAM parameters of Bhuiyan *et al.* [85] and obtained values which, extrapolated down to 1230 K give D close to $1.5 \times 10^{-9} m^2/s$. Given that, according to the results shown in Fig. 15, the shell region of a 4-nm Fe NP at 1200 K has a diffusivity similar to extrapolated molten bulk values, one could argue that the shell region is molten or partially molten at 1200 K, while at 600 K it is still solidlike. However, we note that the shell region contains mostly surface atoms, and that surface diffusion is complex at high temperatures [46]. Therefore, further studies are needed to elucidate this point.

C. Comparison with theoretical models

We have compared our simulation results with a semi-infinite mean-field Ising model, an analytical model that includes surface effects and is described in Sec. III A. In Fig. 16, we have compared the bulk and shell magnetizations obtained from the model with the ones from MD-SD simulations for different values of the exchange constant J. As can be seen, the model results are highly sensitive to the value J, but the qualitative behavior of the system is reasonably well reproduced for the three values considered. The thermal behavior of the analytical surface magnetization reproduces the shape of the corresponding MD-SD curve, also displaying an inflexion point at high temperatures, i.e., dM/dT does not show a monotonous decrease. The rapid decrease of surface magnetization is also observed for the surface magnetization of thin films [44].

Figure 17 shows the analytical results of the model presented in Sec. III B and the computational results for different NPs, showing a good qualitative agreement. It can be seen that the rough qualitative behavior of the different magnetizations is well reproduced.

Quantitative agreement is difficult to achieve using mean-field models like the ones in Figs. 16 and 17. As expected, any mean-field model requires an effective J much lower than the one used in our spin Hamiltonian to adjust the critical temperature. Both models show good agreement with our results for $J = 6.5$ meV. In addition, there are non-negligible differences between Ising and Heisenberg models, as expanded below. Nevertheless, these results are usefull in order to test and support the MD-SD results. It is notable how the model manages to reproduce very well the behavior of the different magnetizations as the size of the NP is enlarged. It shows, as well as the MD-SD simulations, that an 8nm diameter nanosphere behaves closely to a bulk system.

The Ising model variations shown above do not offer an accurate quantitative prediction of our magnetization curves. All of them use the mean-field approximation, and only up/down spin states. This is because solving the Heisenberg model in 3D is not trivial, even for periodic boundary conditions. Recent work shows the "phase diagram" for different values of J at first-, second-, and third-NNs (J_1, J_2, J_3) [82]. The frontier for the (π, π, π) antiferromagnetic phase appears at $J_2/J_1 = 2/3 \sim 0.67$. In our case, for the chosen $J(r_{ij})$, this ratio changes with temperature, and it is also affected by strain in the NP but is close to $J_2/J_1 = 0.6$, and $J_3/J_1 = 0$. This puts our system in the ferromagnetic state and, therefore, close to the frontier between the $(0,0,0)$ ferromagnetic and (π, π, π) phases. The (q,q,q) spiral phase is close, but $J_3 > 0$ would be needed to reach that region of the phase diagram. At 10 K, the separation distance between NN spins (d_{nn}) is around $d_{nn} = 0.245$ nm, and the distance between second NN (d_{2nd}) is about $d_{2nd} = 0.285$ nm, resulting in $J_1 = 19.5$ meV and $J_2 = 12.12$ meV, $J_3 = 0$, giving $J_2/J_1 = 0.62$. At 1000 K, $d_{nn} = 0.25$ nm, $d_{2nd} = 0.29$ nm, $J_1 = 19$ meV, $J_2 = 11$ meV, $J_3 = 0$, giving $J_2/J_1 = 0.58$.

As an alternative simple model for magnetization vs temperature, Fig. S3 of the Supplemental Material [51] shows the curve for the "shape" model by Kuz'min [86]. The comparison of the model with our bulk results shows reasonable agreement if one sets the critical temperature to $T_c = 650$ K in the model.

V. CONCLUSIONS

We have performed combined MD and SD simulations on isolated bcc Fe spherical nanoclusters and studied their magnetic properties as a function of temperature and cluster size, in the absence of external magnetic fields. To this aim, we have used a classical spin Hamiltonian coupled to classical MD. The effect of anisotropy is also considered. Our results naturally include lattice expansion, surface stress, and other factors, which are difficult to include in spin lattice models. Our simulations include Fe nanoclusters with up to 23 000 atoms, and bulk simulations with up to 250,000 atoms in the simulation cell. The temperature of the lattice and the spins can be defined without any additional scaling factors [37], as usually required in SLD simulations [24].

Given the complexity of solving 3D magnetic models, simulations including thermal lattice effects, like thermal expansion and lattice strain due to surface effects, can be valuable tools in understanding and predicting the behavior of nanoscale magnetic systems. We find significant differences between our simulations with moving atoms, and simulations with frozen atoms as in most atomistic SD simulations, specially at temperatures above 2/3 of the critical temperature. Recently, lattice relaxation was found to produce significantly larger coercitivity enhancement in NPs than the case of an unrelaxed, fixed lattice [87].

Our results show excellent agreement with experimental measurements of Fe nanoclusters [59]. The magnetization thermal behavior of small clusters is well reproduced and the estimated Curie temperature is also very similar. Total magnetization decreases with increasing temperature and decreasing size and, therefore, the decrease of magnetization with temperature is faster for the smallest clusters. Qualitatively, these results are expected, but they are quantitatively different from the ones in simple semi-analytical mean-field Ising models, even when size and surface effects are considered. Above the Curie temperature we find that magnetization scales with system size as predicted by models assuming SRMO [65].

For temperatures above 1000 K, we observe evidence of possible melting of the shell region, as shown by both diffusivity and radial coordination studies. This is consistent with melting temperature reduction due to finite size and surface effects in nanoclusters, but only occurs well above T_C in our model.

Regarding our bulk simulations, we obtain an estimated Curie temperature close to $T_C = 650$ K for bulk systems. The discrepancy with the experimental value is attributed to the exchange coupling $J(r_{ij})$. Large differences of the reported values of J as a function of pair separation distance are found in the literature and, therefore, fitting the function $J(r_{ij})$ with a different set of *ab initio* calculations results in different magnetization curves. This statement is clearly verified in Fig. 8 where the bulk Curie temperature is well reproduced if a different set of ab-initio data is used to fit the $J(r_{ij})$ function. Our calculations indicate that possible size dependence of $J(r_{ij})$ might lead to significant magnetization changes.

The total NP magnetization can be considered to be the result of an ordered core plus a less ordered outer shell. In fact, simple two-component models provide a reasonable fit to our results. Core magnetization resembles bulk magnetization and, as cluster size increases, dominates the overall magnetization. Shell magnetization is significantly lower than bulk magnetization, as expected due to the reduction of the local coordination number.

We propose a functional form for the magnetization as a function of size and temperature, which has only two free parameters and works extremely well for temperatures below T_C, and for the range of sizes studied, from 2-nm cluster diameter up to bulk conditions.

It is clear that the classical MD-SD simulations presented in this paper still have several limitations, for example, assuming classical continuous spin variables or the fact that exchange, anisotropy, and magnetic moments are the same for surface and core atoms. However, they are expected to contribute to the understanding of magnetism in nanoscale systems, providing quantitative values to compare with experiments for nanocluster magnetization. Among the improvements to be implemented in future studies, it would be interesting to consider the effect of defects in the clusters, such as vacancies, impurities, dislocations and grain boundaries, together with the role of an external magnetic field and dipolar interactions with other nanoclusters.

[1] V. Pierron-Bohnes, A. Tamion, F. Tournus, and V. Dupuis, Magnetism of low-dimension alloys, *Nanoalloys* (Springer, London, 2012), pp. 287–330.

[2] H.-J. Elmers, Ferromagnetic monolayers, Int. J. Mod. Phys. B **9**, 3115 (1995).

[3] S. Bader, E. Moog, and P. Grünberg, Magnetic hysteresis of epitaxially-deposited iron in the monolayer range: A Kerr effect experiment in surface magnetism, J. Magn. Magn. Mater. **53**, L295 (1986).

[4] H.-J. Elmers, J. Hauschild, and U. Gradmann, Critical behavior of the uniaxial ferromagnetic monolayer Fe(110) on W(110), Phys. Rev. B **54**, 15224 (1996).

[5] M. J. Dunlavy and D. Venus, Critical susceptibility exponent measured from Fe/W (110) bilayers, Phys. Rev. B **69**, 094411 (2004).

[6] M. Kaur, J. S. McCloy, W. Jiang, Q. Yao, and Y. Qiang, Size dependence of inter-and intracluster interactions in core–shell iron–iron oxide nanoclusters, J. Phys. Chem. C **116**, 12875 (2012).

[7] O. Iglesias and A. Labarta, Finite-size and surface effects in maghemite nanoparticles: Monte Carlo simulations, Phys. Rev. B **63**, 184416 (2001).

[8] Z. Nedelkoski, D. Kepaptsoglou, L. Lari, T. Wen, R. A. Booth, S. D. Oberdick, P. L. Galindo, Q. M. Ramasse, R. F. Evans, S. Majetich *et al.*, Origin of reduced magnetization and domain formation in small magnetite nanoparticles, Sci. Rep. **7**, 45997 (2017).

[9] R. Skomski, *Simple Models of Magnetism* (Oxford University Press, New York, 2008).

[10] E. C. Stoner and E. Wohlfarth, A mechanism of magnetic hysteresis in heterogeneous alloys, Philos. Trans. R. Soc. London, Ser. A **240**, 599 (1948).

[11] B. Zimmermann, G. Bihlmayer, M. Böttcher, M. Bouhassoune, S. Lounis, J. Sinova, S. Heinze, S. Blügel, and B. Dupé, Comparison of first-principles methods to extract magnetic parameters in ultrathin films: Co/Pt(111), Phys. Rev. B **99**, 214426 (2019).

[12] F. López-Urías and G. Pastor, Exact diagonalization of hubbard clusters at finite temperatures, Eur. Phys. J. D **52**, 159 (2009).

[13] F. Körmann, A. Dick, T. Hickel, and J. Neugebauer, Pressure dependence of the Curie temperature in bcc iron studied by *ab initio* simulations, Phys. Rev. B **79**, 184406 (2009).

[14] V. P. Antropov, M. I. Katsnelson, B. N. Harmon, M. van Schilfgaarde, and D. Kusnezov, Spin dynamics in magnets: Equation of motion and finite temperature effects, Phys. Rev. B **54**, 1019 (1996).

[15] A. Vansteenkiste, J. Leliaert, M. Dvornik, M. Helsen, F. Garcia-Sanchez, and B. Van Waeyenberge, The design and verification of MuMax3, AIP Adv. **4**, 107133 (2014).

[16] S. Fu, W. Cui, M. Hu, R. Chang, M. J. Donahue, and V. Lomakin, Finite-difference micromagnetic solvers with the object-oriented micromagnetic framework on graphics processing units, IEEE Trans. Magn. **52**, 1 (2016).

[17] G. P. Müller, M. Hoffmann, C. Dißelkamp, D. Schürhoff, S. Mavros, M. Sallermann, N. S. Kiselev, H. Jónsson, and S. Blügel, Spirit: Multifunctional framework for atomistic spin simulations, Phys. Rev. B **99**, 224414 (2019).

[18] R. F. Evans, Atomistic spin dynamics, *Handbook of Materials Modeling: Applications: Current and Emerging Materials* (Springer, Cham, 2020), pp. 427–448.

[19] O. Eriksson, A. Bergman, L. Bergqvist, and J. Hellsvik, *Atomistic Spin Dynamics: Foundations and Applications* (Oxford university press, Oxford, 2017).

[20] Y. Zhou, J. Tranchida, Y. Ge, J. Murthy, and T. S. Fisher, Atomistic simulation of phonon and magnon thermal transport across the ferromagnetic-paramagnetic transition, Phys. Rev. B **101**, 224303 (2020).

[21] X. Wu, Z. Liu, and T. Luo, Magnon and phonon dispersion, lifetime, and thermal conductivity of iron from spin-lattice dynamics simulations, J. Appl. Phys. **123**, 085109 (2018).

[22] D. Beaujouan, P. Thibaudeau, and C. Barreteau, Anisotropic magnetic molecular dynamics of cobalt nanowires, Phys. Rev. B **86**, 174409 (2012).

[23] R. F. Evans, W. J. Fan, P. Chureemart, T. A. Ostler, M. O. Ellis, and R. W. Chantrell, Atomistic spin model simulations of magnetic nanomaterials, J. Phys.: Condens. Matter **26**, 103202 (2014).

[24] M. B. Hahn, Temperature in micromagnetism: Cell size and scaling effects of the stochastic Landau-Lifshitz equation, J. Phys. Commun. **3**, 075009 (2019).

[25] S. Westmoreland, R. Evans, G. Hrkac, T. Schrefl, G. Zimanyi, M. Winklhofer, N. Sakuma, M. Yano, A. Kato, T. Shoji *et al.*, Multiscale model approaches to the design of advanced permanent magnets, Scr. Mater. **148**, 56 (2018).

[26] D. Suess, C. Vogler, F. Bruckner, P. Heistracher, F. Slanovc, and C. Abert, Spin torque efficiency and analytic error rate estimates of skyrmion racetrack memory, Sci. Rep. **9**, 1 (2019).

[27] B. Alkadour, B. W. Southern, J. P. Whitehead, and J. van Lierop, Triangular array of iron oxide nanoparticles: Simulation study of intraparticle and interparticle magnetism, Phys. Rev. B **100**, 094416 (2019).

[28] S. Dudarev and P. Derlet, A 'magnetic' interatomic potential for molecular dynamics simulations, J. Phys.: Condens. Matter **17**, 7097 (2005).

[29] P. M. Derlet and S. Dudarev, Million-atom molecular dynamics simulations of magnetic iron, Prog. Mater. Sci. **52**, 299 (2007).

[30] P.-W. Ma, C. H. Woo, and S. L. Dudarev, Large-scale simulation of the spin-lattice dynamics in ferromagnetic iron, Phys. Rev. B **78**, 024434 (2008).

[31] T. Shimada, K. Ouchi, I. Ikeda, Y. Ishii, and T. Kitamura, Magnetic instability criterion for spin–lattice systems, Comput. Mater. Sci. **97**, 216 (2015).

[32] P.-W. Ma, S. L. Dudarev, and J. S. Wróbel, Dynamic simulation of structural phase transitions in magnetic iron, Phys. Rev. B **96**, 094418 (2017).

[33] P.-W. Ma, S. Dudarev, and C. Woo, Spilady: A parallel CPU and GPU code for spin–lattice magnetic molecular dynamics simulations, Comput. Phys. Commun. **207**, 350 (2016).

[34] D. Perera, D. P. Landau, D. M. Nicholson, G. Malcolm Stocks, M. Eisenbach, J. Yin, and G. Brown, Phonon-magnon interactions in body centered cubic iron: A combined molecular and spin dynamics study, J. Appl. Phys. **115**, 17D124 (2014).

[35] D. Perera, D. M. Nicholson, M. Eisenbach, G. M. Stocks, and D. P. Landau, Collective dynamics in atomistic models with coupled translational and spin degrees of freedom, Phys. Rev. B **95**, 014431 (2017).

[36] J. Hellsvik, D. Thonig, K. Modin, D. Iuşan, A. Bergman, O. Eriksson, L. Bergqvist, and A. Delin, General method for atomistic spin-lattice dynamics with first-principles accuracy, Phys. Rev. B **99**, 104302 (2019).

[37] J. Tranchida, S. Plimpton, P. Thibaudeau, and A. P. Thompson, Massively parallel symplectic algorithm for coupled magnetic spin dynamics and molecular dynamics, J. Comput. Phys. **372**, 406 (2018).

[38] T. Kaneyoshi, *Introduction to Amorphous Magnets* (World Scientific Publishing Company, Singapore, 1992).

[39] K. Yosida, D. C. Mattis, and K. Yosida, *Theory of Magnetism: Edition en anglais*, Vol. 122 (Springer Science & Business Media, Berlin, 1996).

[40] M. Pajda, J. Kudrnovsky, I. Turek, V. Drchal, and P. Bruno, *Ab initio* calculations of exchange interactions, spin-wave stiffness constants, and Curie temperatures of Fe, Co, and Ni, Phys. Rev. B **64**, 174402 (2001).

[41] S. Morán, C. Ederer, and M. Fähnle, *Ab initio* electron theory for magnetism in Fe: Pressure dependence of spin-wave energies, exchange parameters, and Curie temperature, Phys. Rev. B **67**, 012407 (2003).

[42] R. F. Sabiryanov and S. S. Jaswal, Magnons and Magnon-Phonon Interactions in Iron, Phys. Rev. Lett. **83**, 2062 (1999).

[43] W. B. Nurdin and K.-D. Schotte, Dynamical temperature for spin systems, Phys. Rev. E **61**, 3579 (2000).

[44] R. Garibay-Alonso, J. Dorantes-Dávila, and G. M. Pastor, Temperature-dependent magnetic properties of ultrathin Fe films: Interplay between local environment and itinerant ferromagnetism, Phys. Rev. B **73**, 224429 (2006).

[45] J. L. García-Palacios and F. J. Lázaro, Langevin-dynamics study of the dynamical properties of small magnetic particles, Phys. Rev. B **58**, 14937 (1998).

[46] H. Chamati, N. Papanicolaou, Y. Mishin, and D. Papaconstantopoulos, Embedded-atom potential for Fe and its application to self-diffusion on Fe (1 0 0), Surf. Sci. **600**, 1793 (2006).

[47] B. D. Cullity and C. D. Graham, *Introduction to Magnetic Materials* (John Wiley & Sons, New Jersey, 2011).

[48] U. Nowak, O. N. Mryasov, R. Wieser, K. Guslienko, and R. W. Chantrell, Spin dynamics of magnetic nanoparticles: Beyond Brown's theory, Phys. Rev. B **72**, 172410 (2005).

[49] G. M. Pastor, J. Dorantes-Dávila, S. Pick, and H. Dreyssé, Magnetic Anisotropy of *3d* Transition-Metal Clusters, Phys. Rev. Lett. **75**, 326 (1995).

[50] M. Ellis and R. Chantrell, Switching times of nanoscale FePt: Finite size effects on the linear reversal mechanism, Appl. Phys. Lett. **106**, 162407 (2015).

[51] See Supplemental Material at https://link.aps.org/supplemental/10.1103/PhysRevB.xx.xxxxxx for additional figures and movies.

[52] A. Stukowski, Visualization and analysis of atomistic simulation data with OVITO–the open visualization tool, Modell. Simul. Mater. Sci. Eng. **18**, 015012 (2009).

[53] D. Mills, Surface effects in magnetic crystals near the ordering temperature, Phys. Rev. B **3**, 3887 (1971).

[54] D. S. Bertoldi, E. M. Bringa, and E. N. Miranda, Analytical solution of the mean field Ising model for finite systems, J. Phys.: Condens. Matter **24**, 226004 (2012).

[55] D. S. Bertoldi, E. M. Bringa, and E. N. Miranda, Exact solution of the two-level system and the Einstein solid in the microcanonical formalism, Eur. J. Phys. **32**, 1485 (2011).

[56] O. Hovorka, S. Devos, Q. Coopman, W. Fan, C. Aas, R. Evans, X. Chen, G. Ju, and R. Chantrell, The Curie temperature distribution of fept granular magnetic recording media, Appl. Phys. Lett. **101**, 052406 (2012).

[57] J. Yin, M. Eisenbach, D. M. Nicholson, and A. Rusanu, Effect of lattice vibrations on magnetic phase transition in bcc iron, Phys. Rev. B **86**, 214423 (2012).

[58] H. Stanley, *Introduction to Phase Transitions and Critical Phenomena the International Series of Monographs on Physics* (Oxford University Press Inc., Oxford and New York, 1971).

[59] I. M. L. Billas, J. A. Becker, A. Châtelain, and W. A. de Heer, Magnetic Moments of Iron Clusters with 25 to 700 Atoms and Their Dependence on Temperature, Phys. Rev. Lett. **71**, 4067 (1993).

[60] A. V. Ruban and O. E. Peil, Impact of thermal atomic displacements on the Curie temperature of *3d* transition metals, Phys. Rev. B **97**, 174426 (2018).

[61] L. Bergqvist and A. Bergman, Realistic finite temperature simulations of magnetic systems using quantum statistics, Phys. Rev. Mater. **2**, 013802 (2018).

[62] D. Böttcher, A. Ernst, and J. Henk, Temperature-dependent Heisenberg exchange coupling constants from linking electronic-structure calculations and monte carlo simulations, J. Magn. Magn. Mater. **324**, 610 (2012).

[63] A. Szilva, M. Costa, A. Bergman, L. Szunyogh, L. Nordström, and O. Eriksson, Interatomic Exchange Interactions for Finite-Temperature Magnetism and Nonequilibrium Spin Dynamics, Phys. Rev. Lett. **111**, 127204 (2013).

[64] G. M. Pastor, J. Dorantes-Dávila, and K. H. Bennemann, Size and structural dependence of the magnetic properties of small *3d*-transition-metal clusters, Phys. Rev. B **40**, 7642 (1989).

[65] G. M. Pastor and J. Dorantes-Dávila, Short-range magnetic order in Fe$_N$ and Ni$_N$ clusters, Phys. Rev. B **52**, 13799 (1995).

[66] M. Fisher, in *Critical phenomena*, edited by M. S. Green (Academic, New York/London), p. 1.

[67] V. Privman, *Finite Size Scaling and Numerical Simulation of Statistical Systems* (World Scientific Singapore, 1990).

[68] C. Holm and W. Janke, Critical exponents of the classical three-dimensional Heisenberg model: A single-cluster Monte Carlo study, Phys. Rev. B **48**, 936 (1993).

[69] E. Brézin and J. Zinn-Justin, Finite size effects in phase transitions, Nucl. Phys. B **257**, 867 (1985).

[70] J. C. Le Guillou and J. Zinn-Justin, Critical exponents from field theory, Phys. Rev. B **21**, 3976 (1980).

[71] J. Le Guillou and J. Zinn-Justin, Accurate critical exponents from the ε-expansion, J. Phys. Lett. **46**, 137 (1985).

[72] X. Tao, D. P. Landau, T. C. Schulthess, and G. M. Stocks, Spin Dynamics Simulations of BCC Iron: Spin Dynamics Simulations, Phys. Rev. Lett. **95**, 087207 (2005).

[73] E. M. Haines, R. Clauberg, and R. Feder, Short-Range Magnetic Order Near the Curie Temperature Iron from Spin-Resolved Photoemission, Phys. Rev. Lett. **54**, 932 (1985).

[74] J. Dorantes-Dávila, G. Pastor, and K. Bennemann, Calculation of short range magnetic order in iron, Solid State Commun. **59**, 159 (1986).

[75] B. Martinez and R. Camley, Quantum study of the spin wave spectrum of a superlattice with ferromagnetic interfacial coupling, J. Phys.: Condens. Matter **4**, 5001 (1992).

[76] G. Xiao, C. Chien, and M. Natan, Magnetization and its temperature dependence in compositionally modulated amorphous Fe70B30-Ag films, J. Appl. Phys. **61**, 4314 (1987).

[77] A. Corciovei, Spin-wave theory of ferromagnetic thin films, Phys. Rev. **130**, 2223 (1963).

[78] J.-H. Park, E. Vescovo, H.-J. Kim, C. Kwon, R. Ramesh, and T. Venkatesan, Magnetic Properties at Surface Boundary of a Half-Metallic Ferromagnet La$_{0.7}$Sr$_{0.3}$MnO$_3$, Phys. Rev. Lett. **81**, 1953 (1998).

[79] D. Zhao, F. Liu, D. L. Huber, and M. G. Lagally, Magnetization on rough ferromagnetic surfaces, Phys. Rev. B **62**, 11316 (2000).

[80] L. B. Pártay, On the performance of interatomic potential models of iron: Comparison of the phase diagrams, Comput. Mater. Sci. **149**, 153 (2018).

[81] F. Ding, A. Rosén, and K. Bolton, Size dependence of the coalescence and melting of iron clusters: A molecular-dynamics study, Phys. Rev. B **70**, 075416 (2004).

[82] P. Ghosh, T. Müller, F. P. Toldin, J. Richter, R. Narayanan, R. Thomale, J. Reuther, and Y. Iqbal, Quantum paramagnetism and helimagnetic orders in the Heisenberg model on the body centered cubic lattice, Phys. Rev. B **100**, 014420 (2019).

[83] J.-W. Jang, J. Kwon, and B.-J. Lee, Effect of stress on self-diffusion in bcc Fe: An atomistic simulation study, Scr. Mater. **63**, 39 (2010).

[84] R. Gosh, I. M. Syed, Z. Amin, and G. Bhuiyan, A comparative study on temperature dependent diffusion coefficient of liquid Fe, Phys. B: Condens. Matter **426**, 127 (2013).

[85] G. M. Bhuiyan, M. Silbert, and M. J. Stott, Structure and thermodynamic properties of liquid transition metals: An embedded-atom-method approach, Phys. Rev. B **53**, 636 (1996).

[86] M. D. Kuz'min, Shape of Temperature Dependence of Spontaneous Magnetization of Ferromagnets: Quantitative Analysis, Phys. Rev. Lett. **94**, 107204 (2005).

[87] E. A. Velásquez, J. Mazo-Zuluaga, E. Tangarife, and J. Mejía-López, Structural relaxation and crystalline phase effects on the exchange bias phenomenon in FeF_2/Fe core/shell nanoparticles, Adv. Mater. Inter. **7**, 2000862 (2020).

[88] toko.uncu.edu.ar.

[89] http://dirac.df.uba.ar.